Journal of Quantitative Spectroscopy & Radiative Transfer 114 (2013) 91–100

Contents lists available at SciVerse ScienceDirect

Journal of Quantitative Spectroscopy & Radiative Transfer

journal homepage: www.elsevier.com/locate/jqsrt

Uncertainty and interpretation of aerosol remote sensing due to vertical inhomogeneity

Peng-Wang Zhai [a,*], Yongxiang Hu [b], Chris A. Hostetler [b], Brian Cairns [c], Richard A. Ferrare [b], Kirk D. Knobelspiesse [c], Damien B. Josset [a], Charles R. Trepte [b], Patricia L. Lucker [a], Jacek Chowdhary [c]

[a] SSAI, 1 Enterprise Parkway, Suite 200, Hampton, VA, USA
[b] MS 475 NASA Langley Research Center, Hampton, VA 23681-2199, USA
[c] NASA Goddard Institute for Space Studies, New York, NY, USA

ARTICLE INFO

Article history:
Received 29 June 2012
Received in revised form
7 August 2012
Accepted 10 August 2012
Available online 23 August 2012

Keywords:
Remote sensing
Radiative transfer
Aerosol
Polarization

ABSTRACT

We have built an aerosol retrieval algorithm which combines the Look Up Table (LUT) and least squares fitting methods. The algorithm is based on the multi-angle multi-wavelength polarized reflectance at the Top Of the Atmosphere (TOA) measured by the Research Scanning Polarimeter (RSP). The aerosol state parameters are the aerosol particle effective radius, effective variance, complex index of refraction, and aerosol column number density. Monomodal aerosol size distribution is assumed. The Cost Function (CF) of the least squares fitting is designed in consideration of the RSP instrumental characteristics. The aerosol retrieval algorithm inherently assumes one layer of aerosols within the atmosphere. Synthetic polarized radiance data at the TOA have been created assuming either one or two layers of aerosols using the vector radiative transfer code based on successive order of scattering method. Test cases for one-layer aerosol systems show great performance. Around 90% of the total 1200 test cases have CF values smaller than 50. For these cases, the correlation coefficients of the input and retrieved parameters are generally around or larger than 0.98. The effective variance is slightly worse with the correlation coefficient of 0.76938. On the other hand, test cases for two-layer aerosol systems show that only 50% of the total (also 1200) tested cases have final CFs smaller than 50. Among these successful cases ($CF \leq 50$), the retrieved optical depth can still be interpreted as the total column optical depth, though the correlation coefficient is decreased in comparison with the one-layer aerosol cases. We propose to interpret other retrieved aerosol parameters as the average of corresponding parameters for each layer weighted by its optical depth at 865 nm. The retrieved effective radius and complex refractive index can be explained by this scheme (correlation coefficient around 0.9). The effective variance, however, shows decreased performance with the correlation coefficient of 0.46421. This may be due to the strong nonlinearity dependence of the scattering properties on the effective variance.

© 2012 Elsevier Ltd. All rights reserved.

1. Introduction

The Earth's climate is affected by the radiative forcing associated with various sources, including total solar irradiance, the absorption of greenhouse gases (GHG), and scattering by cloud and aerosol particles. Among

* Corresponding author. Tel.: +1 757 864 6288.
E-mail address: pengwang.zhai-1@nasa.gov (P.-W. Zhai).

0022-4073/$ - see front matter © 2012 Elsevier Ltd. All rights reserved.
http://dx.doi.org/10.1016/j.jqsrt.2012.08.006

these sources the aerosol radiative forcing is one of the leading factors whose magnitude is comparable with that of GHG. The uncertainty of aerosol radiative forcing is far greater than that of the GHG [1]. Part of the reason for this is the lack of global aerosol measurements of sufficient content and quality: the number of required aerosol parameters exceeds the number of observables from the current generation of sensors. Ideally, the aerosol shape and size distribution, composition, spectral index of refraction, and spatial distribution of aerosol concentration throughout the atmosphere should be known to accurately model the aerosol radiative forcing. In order to do meaningful retrievals on a few important aerosol parameters, one normally has to assume prescribed conditions. The number of predetermined conditions and specific ways to implement them depends on the types of satellite platforms and the difference between the numbers of unknown parameters and satellite observables. Each of these assumptions will inevitably cause some uncertainties on the aerosol retrievals. It is very important to quantify these uncertainties through theoretical and experimental analysis in order to understand and properly use the satellite aerosol data products. There are many research efforts devoted to this subject, for instance, Refs. [2–4], and the references within.

There are two types of satellite observation instruments: active and passive. Active systems use active electromagnetic wave sources and measure signals backscattered from targets. The Cloud-Aerosol Lidar and Infrared Pathfinder Satellite Observations (CALIPSO), one of the most successful missions of this type, is equipped with a backscatter lidar working at two wavelengths (0.532 μm and 1.064 μm). Cloudsat, another active satellite mission, employs a radar system at 94 GHz mainly targeting clouds and precipitation. Active systems have the unique capability of obtaining vertical distribution information of aerosol or cloud particles. Passive systems, on the other hand, measure either the scattered solar light or thermal emission at the TOA. Notable instruments of this type include the MODerate resolution Imaging Spectroradiometer (MODIS), Multi-angle Imaging SpectroRadiometer (MISR), POLarization and Directionality of the Earth's Reflectances (POLDER), and Aerosol Polarimetry Sensor (APS) onboard the Glory satellite.[1]

The four representative passive instruments show a progressive trend of including multi-angle and polarimetry capability to satellite remote sensors. The MODIS measures radiance at the top of the atmosphere at one viewing angle with wide spectral coverage. The MISR instrument observes the radiance at four wavelength bands with added multi-angle viewing capabilities. The POLDER has multispectral bands, polarization capability at three wavelengths, and multi-angle coverages. Last but not least, the APS measures the linearly polarized radiances (Stokes parameters I, Q, U) at wide spectral range at as many as 250 viewing angles. The Research Scanning Polarimetry (RSP) [5] is the airborne version of the APS, which can be used to explore the advantages and potential of the environmental remote sensing combining multispectral, multi-angle, polarimetry measurements. The RSP takes measurements at nine wavelengths of 0.41027, 0.46913, 0.55496, 0.67001, 0.86351, 0.96, 1.59351, 1.88 and 2.26351 μm. The scanning range of the RSP is $\pm 60^\circ$ from the nadir, and the instantaneous field of view (IFOV) is 14 mrad.

The radiance acquired by passive sensors at the TOA is the integration of scattered light from the whole column of atmosphere. Normally, it is very difficult to get the vertical distribution of aerosol properties from passive sensors. Due to the limitation of passive sensors, the aerosol vertical distribution is often prescribed as a single layer in aerosol remote sensing algorithms [6–9]. In reality there are often situations where multilayer aerosol distribution is present [10–12]. Fig. 1 shows an example of the aerosol extinction and lidar ratio (ratio between the extinction and backscatter coefficients) vertical profiles measured by the NASA Langley High Spectral Resolution Lidar (HSRL) on August 2, 2007 over the Atlantic ocean to the east of Norfolk, VA, USA. The case shown in Fig. 1 has been described in greater details in [12] (see Fig. 7). The extinction and lidar ratio profiles clearly indicate two layers of aerosols in the atmosphere. The lidar ratio profile, containing information on aerosol type, shows that the two layers of aerosols are of different aerosol types. Indeed, they are a smoke layer originating from forest fires in Montana and Idaho, aloft above urban aerosols near the surface. Questions arise naturally when retrievals that assume a single aerosol layer with vertically uniform optical properties are applied to scenes exhibiting multiple aerosol layers of different types:

> Question I: Can the aerosol retrieval algorithm be used to retrieve aerosol properties for a multi-layer aerosol system? If yes, what is the uncertainty introduced by this underlying assumption?

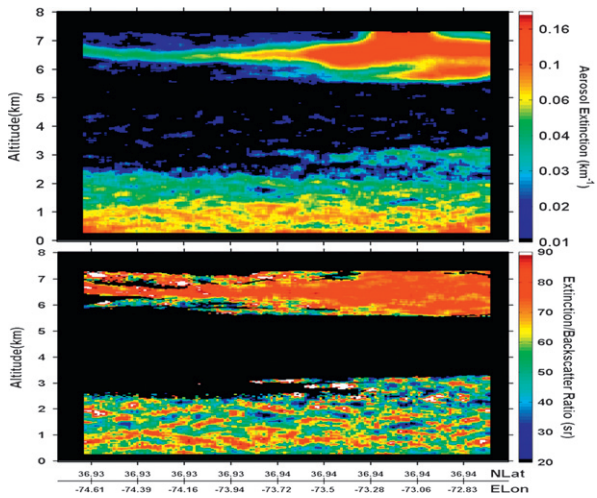

Fig. 1. Layered aerosol distribution taken by the NASA HSRL over the Atlantic ocean at east of Norfolk, VA, USA on August 2, 2007.

[1] The Glory satellite unfortunately failed to reach orbit on March 4, 2011.

Question II: How to interpret the retrieved aerosol properties in terms of the true aerosol optical properties?

This paper addresses both of these questions. We have developed an aerosol retrieval algorithm based on the measurements of the RSP. The algorithm assumes that the aerosol is located in a single layer. A set of cases with two layers of aerosols is simulated by the Vector Radiative Transfer (VRT) code based on the successive order of scattering (SOS) method [13,14]. The polarized radiances for these two-layer cases are used by the aerosol retrieval algorithm to get retrieved aerosol parameters, which are compared with the input aerosol parameters to study and interpret the retrieved parameters and associated uncertainties. One caveat in our aerosol retrieval algorithm is that the monomodal size distribution is assumed for aerosol. This does not affect our analysis within the problem defined. Also the fact is that one mode generally dominates and that it is that mode which will dominate the retrieved microphysics [15].

There are a few studies on remote sensing uncertainty due to vertical inhomogeneity, mostly focusing on the cloud parameter retrieval and polarization information is not included [16–19]. Recently Ref. [20] presented a sensitivity study on aerosol remote sensing using multi-angle polarimetry at a single wavelength (0.446 μm). No retrieval algorithm performance was evaluated in Ref. [20]. In this paper we adopt a more comprehensive method to evaluate aerosol remote sensing uncertainty with a retrieval algorithm based on the RSP instrument. This paper is organized in the following way: Section 2 describes the method we used in this study; Section 3 shows the results and discussion; and finally, Section 4 presents the summary and conclusions.

2. Methodology

The methodology can be described in the following three steps:

Step I: An aerosol retrieval algorithm is built with the assumption that the aerosol is distributed in a single layer. The inputs of the retrieval algorithm are the RSP or APS observables, which are the reflected Stokes parameters *I*, *Q*, *U* at the TOA at multiple observation angles and wavelengths. The outputs are the aerosol state vector composed of the effective radius and variance of the size distribution, the complex refractive index, and aerosol column number density. The optical depth at any wavelength can be derived from these parameters.

Step II: The observables for cases with multi-layer aerosols are generated by the SOS VRT model. These observables are then used as inputs to the aerosol retrieval algorithm to derive retrieved aerosol parameters.

Step III: The retrieved aerosol parameters are compared with the true aerosol parameters to answer the questions posed in the introduction.

In practice, the Stokes parameters measured by the RSP are scaled by the incident solar irradiance F_0:

$$R_I = \frac{I\pi r_0^2}{F_0 \cos\theta_s}, \quad R_Q = \frac{Q\pi r_0^2}{F_0 \cos\theta_s}, \quad R_U = \frac{U\pi r_0^2}{F_0 \cos\theta_s}, \tag{1}$$

where r_0 is the solar distance in AU and θ_s is the solar zenith angle. The quantities R_I, R_Q, and R_U are the functions of wavelength, the solar/viewing geometry, and aerosol state vectors, respectively. We choose the RSP scanning plane that coincides with the solar principle plane, i.e., the plane formed by the solar incident and local zenith directions. The main consideration is that the scattering angle range is the largest by this choice. In addition, $R_U=0$ in the principle plane, which simplifies some computational aspects. The viewing angle resolution used in this work is $1^\circ \approx 17.45$ mrad, i.e., a total number of $2\times 60+1=121$ viewing angles are used within the range of $\pm 60^\circ$. The angular resolution of the RSP is 14 mrad which is slightly finer than that used here. The RSP has nine wavelengths ranging from 0.41027 μm to 2.26351 μm. We use three wavelengths in this retrieval, 0.41027 μm, 0.67001 μm, and 2.26351 μm, to simplify the computation burden while maintaining the ability to retrieve aerosol size information. In this study we use the VRT model to simulate the observables of the RSP instrument as inputs to the retrieval algorithm. Inevitably, measurement errors are always associated with real measurements from instruments. In order to study the uncertainty due to the vertical distribution assumption, we need to minimize the random or systematic measurement errors. Using synthetic simulation data from accurate VRT model achieves this purpose. In addition, the aerosol information used in the simulation can be further employed to do comparison with the retrieved aerosol information, by which the retrieval uncertainty can be assessed.

The aerosol retrieval algorithm is based on the Levenberg–Marquardt algorithm [21,22] for least squares fitting to minimize the following Cost Function (CF):

$$\Phi = \sqrt{\sum_i \left(\frac{[R_I^l(i)-R_I^m(i)]^2}{C_I^m(i)} + \frac{[R_Q^l(i)-R_Q^m(i)]^2}{C_Q^m(i)} \right)} \tag{2}$$

where the superscript m and l are used to denote the input and fitted reflectances, respectively; C_I^m and C_Q^m are the error covariance for R_I and R_Q, respectively [23,15]

$$C_I^m(i) = 10^{-7} \cos\theta_s R_I^m(i) + [0.03 R_I^m(i)]^2, \tag{3a}$$

$$C_Q^m(i) = 10^{-7} \cos\theta_s R_I^m(i) + [0.03 R_Q^m(i)]^2 + \{0.001[R_I^m(i) + |R_Q^m(i)|]\}^2, \tag{3b}$$

and i is used to denote the functional dependence on wavelengths, scanning angle, and aerosol state vectors. The error covariance C_I^m and C_Q^m are designed to conform the instrumental characteristics of the RSP [23,15]. As we have emphasized before, $R_U^m = 0$ in the principle plane and the input field R_I^m and R_Q^m are generated by the VRT model in accordance with the RSP designs. Eq. (3) are used to take the RSP sensitivities into account.

For the description of the aerosol state, the monomodal log-normal size distribution is used

$$N(r) = \frac{n_0}{\sqrt{2\pi}\ln\sigma_g r}\exp\left(\frac{-(\ln r - \ln r_g)^2}{2\ln^2\sigma_g}\right), \tag{4}$$

where n_0 in the unit of m^{-3} is the particle number density; r_g and σ_g are related to r_{eff} and v_{eff} by:

$$r_{eff} = r_g \exp\left(\tfrac{5}{2}\ln^2\sigma_g\right), \tag{5a}$$

$$v_{eff} = \exp(\ln^2\sigma_g) - 1. \tag{5b}$$

The column number density N_0 can be defined for a homogenous aerosol layer with the thickness of δl:

$$N_0 = n_0 \cdot \delta l. \tag{6}$$

The aerosol extinction and scattering optical depths $\tau_{ext,a}$ and $\tau_{scat,a}$ are the products of aerosol cross sections and N_0

$$\tau_{ext,a} = N_0 C_{ext,a}, \quad \tau_{scat,a} = N_0 C_{scat,a}, \tag{7}$$

where $C_{ext,a}$ and $C_{scat,a}$ are the extinction and scattering cross sections, respectively. They are implicit functions of r_{eff}, v_{eff}, m_r, m_i, and incident light wavelength λ. The extinction cross section $C_{ext,a}$, as well as the scattering cross section $C_{scat,a}$ and the aerosol scattering matrix $\mathbf{P}_a$ are calculated by the Mie theory [24,25].

In this work the aerosol state vector contains the aerosol effective radius r_{eff} and variance v_{eff} of the size distribution, the real m_r and imaginary m_i refractive index, and the aerosol column number density N_0. The retrieval algorithm has assumed that aerosol is confined within one homogeneous layer in the altitude range from 0 to 2 km (adjustable if needed). Within the aerosol layer, the light scattering properties are mixed from aerosols and molecules

$$\tau_{ext} = \tau_{ext,a} + \tau_{scat,r}, \tag{8a}$$

$$\tau_{scat} = \tau_{scat,a} + \tau_{scat,r}, \tag{8b}$$

$$\mathbf{P} = \frac{\tau_{scat,a}\mathbf{P}_a + \tau_{scat,r}\mathbf{P}_r}{\tau_{scat}}, \tag{8c}$$

$$\omega = \frac{\tau_{scat}}{\tau_{ext}}, \tag{8d}$$

where the subscripts a and r stand for aerosol and Rayleigh (molecular) scattering, respectively; τ_{scat} and τ_{ext} are the total optical depths due to scattering and extinction, respectively; ω is the overall single scattering albedo; and $\mathbf{P}$ is the scattering matrix. We have assumed that molecular scattering is conservative, i.e., no absorption for molecular scattering. Trace gas absorption is neglected. Above the aerosol layer, the atmosphere is assumed to be a single layer Rayleigh scattering medium.

For a set of virtual measurements R_I^m and R_Q^m, the Levenberg–Marquardt algorithm starts with an initial guess of the aerosol state vector x_0 and calls the VRT model to calculate R_I^l and R_Q^l. The CF Φ is then calculated based on Eq. (2). A perturbation to the state vector x_0 is made based on the Jacobian matrix, which is the derivative of the polarized radiance field with respect to the state vector components. A new set of R_I^l and R_Q^l are calculated using the VRT model based on the new state vector. The CF is then updated with the new R_I^l and R_Q^l. The new state vector is kept/discarded if the CF decreases/increases. If the state perturbation increases or does not decrease the CF, then the perturbation bound is adjusted (usually within 10% of the previous value), and a new perturbation will be calculated. If the number of attempts exceed a threshold value MAXFEV (MAXFEV = 50 is used in this work), the algorithm will be terminated and the retrieval is marked unsuccessful. A convergence test is performed for each iteration based on the difference in the state vectors and CFs for consecutive steps. If a convergence is reached the algorithm will exit the iteration and report the final state vector. The readers are referred to Refs. [21,22] for details of the mathematical aspects of the Levenberg–Marquardt algorithm. Previously Refs. [23,15] have published similar aerosol retrieval algorithms. A few additional examples can be found in Refs. [6,8].

The selection of the initial state vector x_0 is very important for cases with multiple local CF minimum and can reduce the possible number of iterations. We use a Look-Up Table (LUT) method to fulfill this purpose. The LUT is built in terms of optical thicknesses at 555 nm (0.05, 0.1, 0.2, 0.4, 0.8, 1.0), real index of refraction (1.3, 1.38, 1.46, 1.54, 1.62), imaginary index of refraction (0.01, 0.02, 0.04, 0.08, 0.16), effective radius (0.1, 0.2, 0.4, 0.8, 1.6, 3.2), and effective variance of the size distribution (0.1, 0.2, 0.4, 0.8, 1.6). The total number of cases for the LUT is $6 \times 5 \times 5 \times 6 \times 5 = 4500$. For a case to be retrieved, the aerosol state vector with the minimum CF in the LUT is used as the initial guess of the Levenberg–Marquardt algorithm.

The VRT model used in this study is the SOS code developed at the NASA Langley Research Center [13,14]. The original code was designed to solve the VRT for coupled atmosphere and ocean systems. Here we use a simplified version of the code to calculate the vector radiance field for the atmosphere bounded by a black surface, i.e., no lower boundary. The SOS method decomposes the total polarized radiance field into the contributions from different orders of scattering [26,27]. The first order of scattering is predicted exactly. The second or higher order contributions are expressed as successive integrals of optical depth and angular integrations. The SOS code converges fast for cases of thin optical depth or absorptive media. It also works fine for thick optical depth cases due to the geometric series approximation [13]. For phase function with large forward peaks, we use the delta-fit technique to truncate the phase function as well as other phase matrix elements [28,13].

3. Results and discussion

First, the aerosol retrieval algorithm needs to be validated. We use the SOS VRT model to simulate the polarized field R_I^m and R_Q^m for $N_{total} = 1200$ test cases assuming a one-layer aerosol system in the atmosphere. In these test cases, the state vector is specified in the

following way:

$$r_{eff} = r_{min} + \eta_1 * (r_{max} - r_{min}),$$
$$v_{eff} = v_{min} + \eta_2 * (v_{max} - v_{min}),$$
$$m_r = m_{r,min} + \eta_3 * (m_{r,max} - m_{r,min}),$$
$$m_i = m_{i,min} + \eta_4 * (m_{i,max} - m_{i,min}),$$
$$\tau_{865} = \tau_{865,min} + \eta_5 * (\tau_{865,max} - \tau_{865,min}), \quad (9)$$

where $r_{min} = 0.05$ μm, $r_{max} = 3.05$ μm, $v_{min} = 0.05$, $v_{max} = 0.65$, $m_{r,min} = 1.3$, $m_{r,max} = 1.6$, $m_{i,min} = 0$, $m_{i,max} = 0.16$, $\tau_{865,min} = 0$, $\tau_{865,max} = 1.2$, and η_i, $i = 1-5$, are random numbers evenly distributed within the interval of [0,1]. The minimum and maximum values of each quantities are set so that nearly all possible scenarios could be included.

These R_I^m and R_Q^m are then used by the aerosol retrieval algorithm to retrieve aerosol parameters. For an ideal aerosol retrieval algorithm, retrieved parameters should be exactly the same as the input parameters within the VRT code numerical accuracy. However, this may never be achieved due to the local minimum of the CFs and high dimensions of parameter space. Note that the instrumental noise is not included in this work because we use the VRT simulated data as inputs to the aerosol retrieval algorithm. Fig. 2 shows $N(\Phi < \Phi_c)/N_{total}$ as a function of Φ_c, where Φ is the CF evaluated with the retrieved aerosol state vector; Φ_c is a CF filter; $N(\Phi < \Phi_c)$ is the number of cases with $\Phi < \Phi_c$. The interpretation of Fig. 2 is the success rate of the retrieval algorithm as a function of some critical filter. It shows that nearly 80% of the cases have final CF smaller than 20; and around 90% of the total 1200 cases have $\Phi < 50$. The CF at the retrieved aerosol state is a good indicator of how well the polarized radiances are fitted, which in turn shows the validity of the retrieval. Hereafter, we use $\Phi_c = 50$ as a critical filter value to discriminate a successful or failed retrieval.

The comparison of the retrieved and input parameters for all the successful cases ($\Phi < 50$) are plotted in Figs. 3 and 4. Fig. 3 shows the scatter plot of the input and retrieved optical depth at 865 nm as well as the linear fit

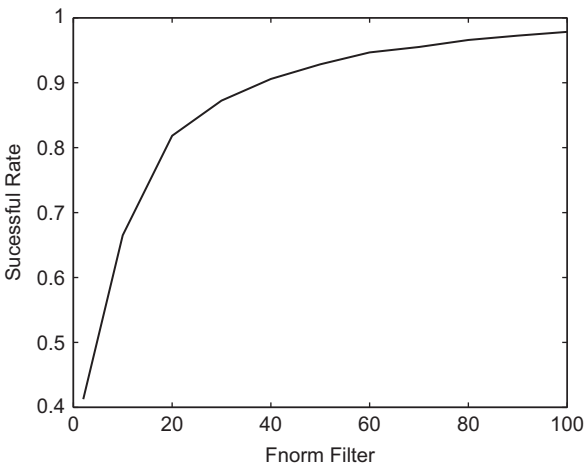

Fig. 2. $N(\Phi < \Phi_c)/N_{total}$ as a function of Φ_c, where Φ is the CF evaluated at the retrieved aerosol state vector; Φ_c is a critical CF filter. The input parameters are assuming an one-layer aerosol, which is the same as the aerosol retrieval algorithm.

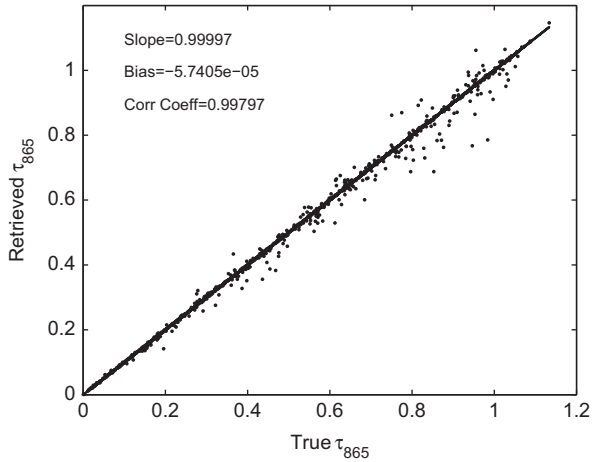

Fig. 3. The comparison of retrieved optical depth at 865 nm with the corresponding true (input) value for single layer aerosol systems.

of the retrieved and input parameter. Note that the 865 nm channel is not used in the current retrieval algorithm. Instead, the optical depth at 865 nm is derived from the basic aerosol state vectors (see Eq. (7)). Later in this paper we will propose an interpretation of the retrieved aerosol parameters for a multi-layered media which uses the optical depth at 865 nm as a weighting function. This is the prime reason of presenting the optical depth at 865 nm. It is also worth noting that 865 nm is close to the geometric mean of the three wavelengths used in this work. The slope and bias are almost perfect (0.99997, and 5.7e−5, respectively); and the correlation coefficient ("Corr Coeff" in the figure) between the input and retrieved optical depth at 865 nm is 0.99797. The size distribution (effective radii and variances) and complex index of refraction for the same cases are plotted in Fig. 4. It is shown that the effective variance has the worst performance among these parameters. The reason is that the aerosol scattering properties are least sensitive to the effective variance, and that the effective variance is correlated with the effective radius in its mathematical definition. Other parameters generally show the correlation coefficients are around or larger than 0.98. The slope and bias are close to 1 and 0, respectively. The results set a base performance standard for one-layer system which will be compared with the two-layer system results.

The next step is to study the uncertainty of the aerosol algorithm due to the vertical layer assumption. We have simulated $N_{total} = 1200$ random cases in which a two-layer aerosol medium is used. The aerosol parameters for each layer are set in a way similar to Eq. (9), with the exception that $\tau_{865,max}$ is now equal to 0.5. This way the total optical depth of the two layers does not exceed 1. The TOA polarized radiance fields are used as inputs to the aerosol retrieval algorithm based on the RSP instrument. The retrieved parameters are then compared with the input parameters to study the uncertainty. Fig. 5 shows the success rate as a function of the CF critical filter Φ_c for the two-layer aerosol cases. It shows that the success rate curve is much flatter than the one in Fig. 2. The number of cases with $\Phi < 50$ is only around 50% of the total tested

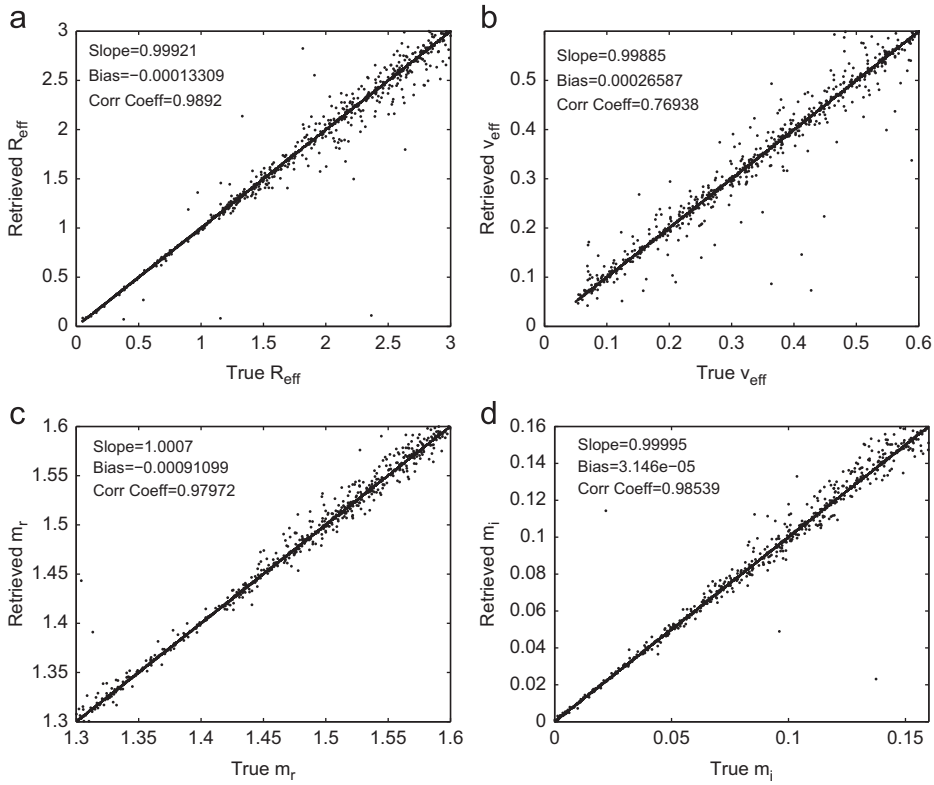

Fig. 4. The comparison of retrieved properties with the corresponding true (input) value for single layer aerosol systems. (a) Effective radius, (b) effective variance, (c) real refractive index, and (d) imaginary refractive index.

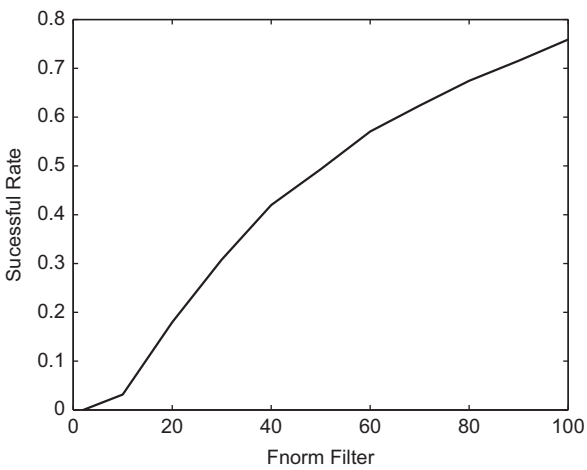

Fig. 5. The same as Fig. 2 except for the two-layer aerosol cases.

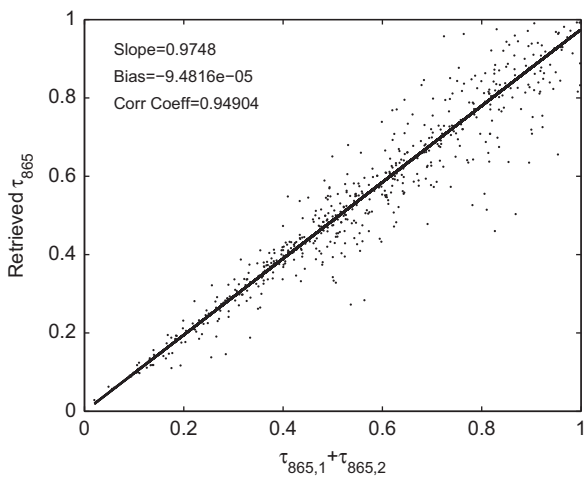

Fig. 6. The comparison of retrieved optical depth at 865 nm with the corresponding true (input) value for two layer aerosol systems.

cases, which is much less than the one-layer cases (more than 90%). This means that the retrieval success rate is generally lower if the vertical layer assumption is not correct. On the other hand, there are 50% of the two-layer aerosol cases which could be fitted by adjusting one-layer aerosol state vector with the final CF smaller than 50.

Fig. 6 shows the total retrieved aerosol optical depth at 865 nm versus the input values for all the successful cases ($\Phi < 50$). The correlation coefficient for this case degrades from 0.99997 (Fig. 3) to 0.94904. The slope and bias are now 0.9748 and $-9.48e-5$, respectively. It is straightforward to compare the input and retrieved total optical depths. However, it is not so easy to interpret other retrieved parameters. How is the retrieved effective radius related to the true input effective radii? What about the index of refraction? To answer this, we need to perform some physical analysis.

For simplicity, we start with the SOS formulas and assume the total radiance field is dominated by the single scattering contribution. The first order radiance vector $\mathbf{L}_1 = (I_1, Q_1, U_1, V_1)$ for the two-layer aerosol system can be written as

$$\mathbf{L}_1 = \int_0^{\tau_{max}} \exp(-\tau'/\mu)\mathbf{S}_1(\tau',\mu,\phi)\, d\tau'/|\mu|, \tag{10}$$

where

$$\mathbf{S}_1(\tau,\mu,\phi) = \frac{\omega(\tau)}{4\pi} \exp(-\tau/|\mu_0|)\mathbf{P}(\tau,\mu,\phi,\mu_0,\phi_0)\mathbf{E}_0 \tag{11}$$

is the first order source function; μ and ϕ are the cosine of viewing zenith and azimuth angle, respectively; μ_0 and ϕ_0 are similar to μ and ϕ but pertain to the solar incident direction; and $\mathbf{E}_0$ is the solar irradiance. The maximum optical depth τ_{max} is the summation of the two layer optical depths $\tau_{max} = \tau_1 + \tau_2$, where τ_1 and τ_2 are the optical depths for the top and bottom layers, respectively. Furthermore, we note $\mathbf{P}(\tau < \tau_1) = \mathbf{P}_1$ and $\mathbf{P}(\tau_1 < \tau < \tau_{max}) = \mathbf{P}_2$. The same rule applies to the single scattering albedo. We have the following equation:

$$\mathbf{L}_1 = \frac{\omega_1}{4\pi}\int_0^{\tau_1} \exp\left[-\tau'\left(\frac{1}{|\mu|}+\frac{1}{|\mu_0|}\right)\right]\mathbf{P}_1\mathbf{E}_0\, d\tau'/|\mu| + \frac{\omega_2}{4\pi}\int_{\tau_1}^{\tau_{max}} \exp\left[-\tau'\left(\frac{1}{|\mu|}+\frac{1}{|\mu_0|}\right)\right]\mathbf{P}_2\mathbf{E}_0\, d\tau'/|\mu|, \tag{12}$$

where the angular dependence for the phase matrices has been made implicit for brevity. The optical depth integration can be evaluated considering that $\mathbf{P}_1$ and $\mathbf{P}_2$ are not a function of the optical depth:

$$\int_0^{\tau_1} \exp\left[-\tau'\left(\frac{1}{|\mu|}+\frac{1}{|\mu_0|}\right)\right]d\tau'/\mu = \frac{|\mu_0|}{|\mu_0|+|\mu|}\left\{1-\exp\left[-\tau_1\left(\frac{1}{|\mu|}+\frac{1}{|\mu_0|}\right)\right]\right\} \tag{13}$$

$$\int_{\tau_1}^{\tau_{max}} \exp\left[-\tau'\left(\frac{1}{|\mu|}+\frac{1}{|\mu_0|}\right)\right]d\tau'/\mu = \frac{|\mu_0|}{|\mu_0|+|\mu|}\left\{\exp\left[-\tau_1\left(\frac{1}{|\mu|}+\frac{1}{|\mu_0|}\right)\right] -\exp\left[-\tau_2\left(\frac{1}{|\mu|}+\frac{1}{|\mu_0|}\right)\right]\right\}. \tag{14}$$

We further use the following small optical depth approximations:

$$\exp\left[-\tau_i\left(\frac{1}{|\mu|}+\frac{1}{|\mu_0|}\right)\right] \approx 1-\tau_i\left(\frac{1}{|\mu|}+\frac{1}{|\mu_0|}\right), \tag{15}$$

where $i=1$, max. The first order radiance vector can be simplified as

$$\mathbf{L}_1 \approx \frac{\omega_1}{4\pi\mu}\mathbf{P}_1\mathbf{E}_0\tau_1 + \frac{\omega_2}{4\pi\mu}\mathbf{P}_2\mathbf{E}_0\tau_2. \tag{16}$$

Under the small optical depth approximation, Eq. (16) shows that the first order radiance vector is a linear combination of the contributions from the two layers, weighted by the optical depth. If we further assume the

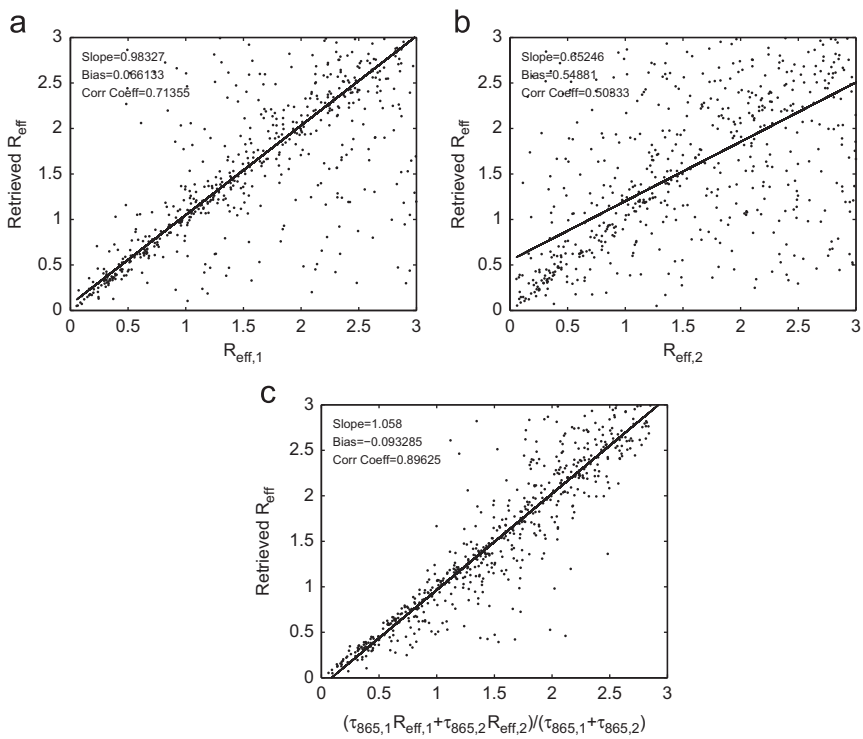

Fig. 7. The comparison of retrieved effective radius with the corresponding true (input) value for two layer aerosol systems. The subscript "1" or "2" denotes the top or bottom layer, respectively.

following linearization relation:

$$f_i(\mathbf{x}) = \omega_i \mathbf{P}_i$$
$$f_i(\mathbf{x}) = f_i'(\mathbf{x}_p)(\mathbf{x}-\mathbf{x}_p) \tag{17}$$

where $\mathbf{x}$ is the state vector and $\mathbf{x}_p$ is some priority state vector; we could generally interpret the retrieved aerosol state vector as the linear combination of the state vector of each layer.

Fig. 7(a)–(c) shows the comparison of the retrieved effective radius R_{eff} with $R_{eff,1}$, $R_{eff,2}$, and $(\tau_{865,1}R_{eff,1}+\tau_{865,2}R_{eff,2})/(\tau_{865,1}+\tau_{865,2})$, respectively. The subscripts 1 and 2 are referring to the top and bottom layers, respectively. For convenience, we here use $Corr(x,y)$ to denote the correlation between variables x and y. It is observed that $Corr(R_{eff},R_{eff,1})$ and $Corr(R_{eff},R_{eff,2})$ are quite small. The correlation $Corr(R_{eff},(\tau_{865,1}R_{eff,1}+\tau_{865,2}R_{eff,2})/(\tau_{865,1}+\tau_{865,2}))=0.89625$, however, is larger than both $Corr(R_{eff},R_{eff,1})=0.71355$ and $Corr(R_{eff},R_{eff,2})=0.50333$. The slope and bias for the linear fit between R_{eff} and $(\tau_{865,1}R_{eff,1}+\tau_{865,2}R_{eff,2})/(\tau_{865,1}+\tau_{865,2})$ are reasonably close to 1 and 0, respectively. This confirms our first order analysis that the retrieved aerosol state vector for multi-layer system can be approximately interpreted as the average of the aerosol states weighted by the optical depth of each layer. Fig. 8(a)–(c) shows the comparison of the retrieved real refractive index m_r with $m_{r,1}$, $m_{r,2}$, and $(\tau_{865,1}m_{r,1}+\tau_{865,2}m_{r,2})/(\tau_{865,1}+\tau_{865,2})$. The same conclusion for the real refractive index could be drawn as the effective radius. In addition, the statistics of imaginary refractive index m_i and effective variance v_{eff} are shown in Fig. 9.

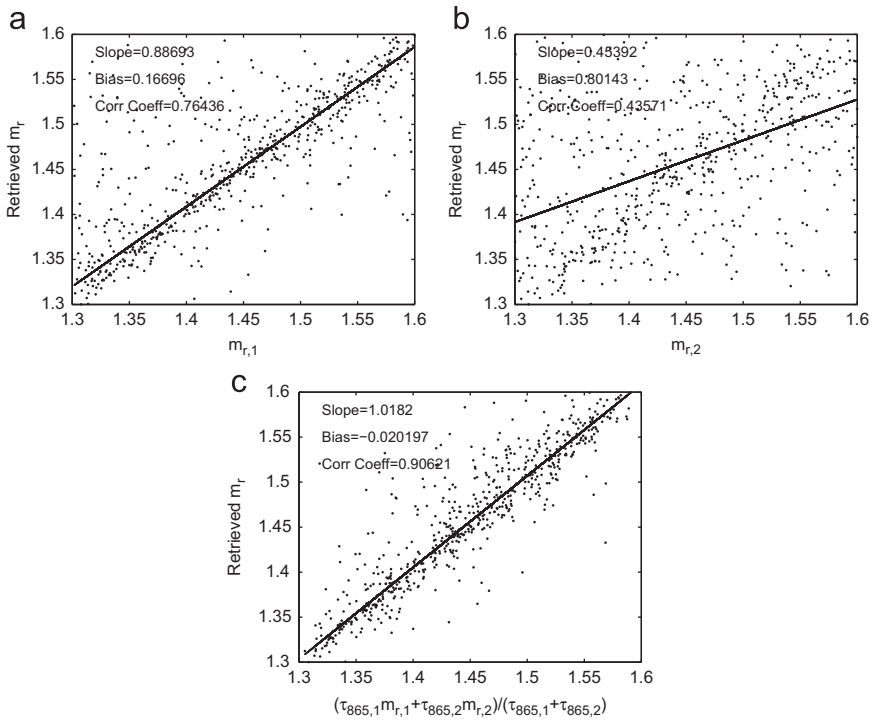

Fig. 8. The same as Fig. 7 except for the real refractive index.

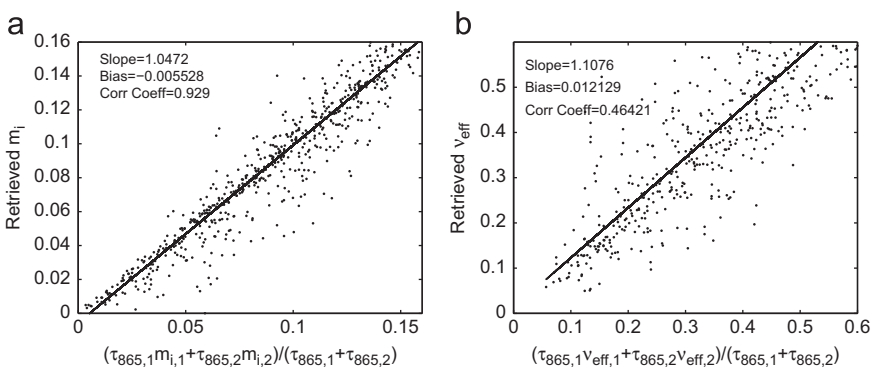

Fig. 9. The comparison of retrieved imaginary refractive index and effective variance with the weighted average of the corresponding parameters for the two aerosol layers used.

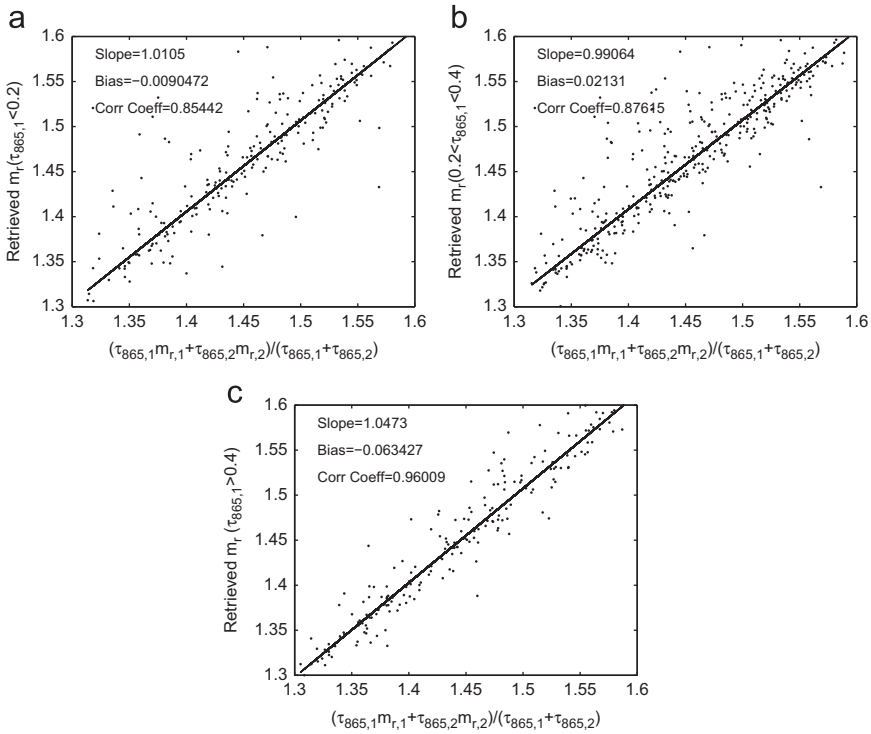

Fig. 10. The relation of retrieved real refractive index with the weighted average of the two layers grouped by the optical depth of the top layer.

The imaginary refractive index shows similar performance as R_{eff} and m_r. The effective variance correlation coefficient, however, is relatively small $Corr(v_{eff},(\tau_{865,1} v_{eff,1}+\tau_{865,2} v_{eff,2})/(\tau_{865,1}+\tau_{865,2}))=0.46421$. Recall from the results for single layer aerosol cases that the effective variance performance is also worse than other parameters. It should be noted that the retrieval of effective variance is tightly interlinked with the effective radius, which makes it a strong nonlinear relationship with the aerosol phase matrix. Readers may refer to Ref. [29] for further discussions on effective variance.

For a two-layer aerosol system, the top layer will contribute to the total radiance more directly, while the bottom layer has to undergo attenuation from the top layer. Therefore, it should be expected that the bottom layer effect should be less if the top layer optical depth is larger. In other words, the inhomogeneity effect will be less as the top layer optical depth increases. Fig. 10 shows the statistics of real index of refraction grouped by the top layer optical depth. Fig. 10(a)–(c) is for the top layer optical depth at 865 nm less than 0.2, between 0.2 and 0.4, and larger than 0.4, respectively. The correlation coefficient is larger for the larger optical depth group, which meets our expectations.

4. Summary

We have studied the uncertainty and interpretation of the aerosol retrieval for multi-layer aerosol systems. The aerosol retrieval algorithm uses reflectance data measured by the RSP. The scanning plane of the RSP coincides with the solar principle plane. Viewing angle zenith angle is in the range of $\pm 60^\circ$. Three wavelengths are used, which are 0.41027 μm, 0.67001 μm, and 2.26351 μm. The aerosol state vector is composed of the aerosol particle effective radius, effective variance, complex index of refraction, and aerosol column number density. Other aerosol parameters can be derived from these five free parameters. The Levenberg–Marquardt algorithm for the least squares fitting technique is used for fitting the polarized reflectance at the TOA by adjusting the aerosol state vector. The aerosol retrieval algorithm assumes a one-layer aerosol in the atmosphere. Two sets of test cases calculated by the VRT model are used to test the aerosol algorithm; one set assumes one-layer aerosols and the other assumes two-layer aerosols. For polarized reflectance for one-layer aerosol systems, the aerosol retrieval algorithm shows great performance. Nearly 90% of the one-layer test cases have the CFs for the retrieved aerosol state vector smaller than 50. The correlation between the input and retrieved aerosol parameters for these cases ($CF \leq 50$) are generally around or higher than 0.98, with the exception of effective variance (correlation is 0.76938 between the input and retrieved effective variance). On the other hand, only 50% of the two-layer test cases have CFs for the retrieved aerosol state vector smaller than 50. Among the successful cases ($CF \leq 50$), the retrieved optical depth at 865 nm can still be closely related to the total input optical depth at 865 nm with the correlation coefficient equal to 0.949. The other retrieved parameters, however, have to be interpreted as the average of the corresponding aerosol parameters of each layer, weighted by the optical depth. The effective variance has the worst performance due to the strong nonlinearity dependence of the scattering properties on the effective

variance. The top layer has larger impacts on the retrieved parameters. This study could help to understand the aerosol retrieval for complex multi-layer systems and assess the uncertainty due to this complexity.

Acknowledgments

This study is supported by the NASA Radiation Science program administrated by Hal Maring and the Biogeochemistry program administrated by Paula Bontempi.

References

[1] Hansen J, Nazarenko L, Ruedy R, Sato M, Willis J, Genio AD, et al. Earth's energy imbalance: confirmation and implications. Science 2005;308:1431–5.
[2] Kokhanovsky AA, Deuzé JL, Diner DJ, Dubovik O, Ducos F, Emde C, et al. The inter-comparison of major satellite aerosol retrieval algorithms using simulated intensity and polarization characteristics of reflected light. Atmos Meas Tech 2010;3:909–32.
[3] Mishchenko MI, Liu L, Geogdzhayev IV, Travis LD, Cairns B, Lacis AA. Toward unified satellite climatology of aerosol properties. 3. MODIS versus MISR versus AERONET. J Quant Spectrosc Radiat Transfer 2010;111:540–52.
[4] Kahn RA, Garay MJ, Nelson DL, Levy RC, Bull MA, Diner DJ, et al. Response to 'Toward unified satellite climatology of aerosol properties. 3. MODIS versus MISR versus AERONET'. J Quant Spectrosc Radiat Transfer 2011;112:901–9.
[5] Cairns B, Travis LD, Russel EE. The Research Scanning Polarimeter: calibration and ground-based measurements. In: Proceedings of SPIE, vol. 3745; 1999. p. 186–96.
[6] Chowdhary J, Cairns B, Mishchenko MI, Travis LD. Retrieval of aerosol properties over the ocean using multispectral and multi-angle photopolarimetric measurements from the Research Scanning Polarimeter. Geophys Res Lett 2001;28:243–6.
[7] Levy RC, Remer LA, Tanré D, Mattoo S, Kaufman YJ. Algorithm for remote sensing of tropospheric aerosol over dark targets from MODIS: Collections 005 and 051: Revision 2, MODIS Algorithm Theoretical Basis Document (MOD04). 〈http://modis-atmos.gsfc.nasa.gov/_docs/ATBD_MOD04_C005_rev2.pdf〉; 2009.
[8] Diner DJ, Hodos RA, Davis AB, Garay MJ, Martonchik JV, Sanghavi SV, von Allmen P, Kokhanovsky AA, Zhai P. An optimization approach for aerosol retrievals using simulated MISR radiances. Atmos Res 2012;116:1–14.
[9] Dubovik O, Herman M, Holdak A, Lapyonok T, Tanré D, Deuzé JL, et al. Statistically optimized inversion algorithm for enhanced retrieval of aerosol properties from spectral multi-angle polarimetric satellite observations. Atmos Meas Tech 2011;4:975–1018.
[10] Soriano C, Rocadenbosch F, Puente C, Rodríguez A, Baldasano JM, Comerón A. Confirmation of a multilayer arrangement of aerosols in the Barcelona air basin using two independent lidar systems. In: Schäfer K, editor. Spectroscopic atmospheric environmental monitoring techniques, vol. 3593. SPIE Proceedings Series; 1998. p. 212–22.
[11] Johnson BT, Heese B, McFarlane SA, Chazette P, Jones A, Bellouin N. Vertical distribution and radiative effects of mineral dust and biomass burning aerosol over West Africa during DABEX. J Geophys Res 2008;113:D00C12. http://dx.doi.org/10.1029/2008JD009848.
[12] Burton SP, Ferrare RA, Hostetler CA, Hair JW, Rogers RR, Obland MD, et al. Aerosol classification using airborne High Spectral Resolution Lidar measurements—methodology and examples. Atmos Meas Tech Discuss 2011;4:5631–88.
[13] Zhai P, Hu Y, Trepte CR, Lucker PL. A vector radiative transfer model for coupled atmosphere and ocean systems based on successive order of scattering method. Opt Express 2009;17:2057–79.
[14] Zhai P, Hu Y, Chowdhary J, Trepte CR, Lucker PL, Josset DB. A vector radiative transfer model for coupled atmosphere and ocean systems with a rough interface. J Quant Spectrosc Radiat Transfer 2010;111:1025–40.
[15] Knobelspiesse K, Cairns B, Ottaviani M, Ferrare R, Hair J, Hostetler CA, et al. Combined retrievals of boreal forest fire aerosol properties with a polarimeter and lidar. Atmos Chem Phys Discuss 2011;11:7909–69. http://dx.doi.org/10.5194/acpd-11-7909-2011.
[16] Nakajima T, King MD. Determination of the optical thickness and effective particle radius of clouds from reflected solar radiation measurements. Part I: TheoryJ Atmos Sci 1990;47:1878–93.
[17] Platnick S. Vertical photon transport in cloud remote sensing problems. J Geophys Res 1990;105:22919–35.
[18] Yang P, Gao B, Baum BA, Wiscombe WJ, Hu Y, Nasiri SL, et al. Sensitivity of cirrus bidirectional reflectance to vertical inhomogeneity of ice crystal habits and size distributions for two moderate-resolution imaging spectroradiometer (MODIS) bands. J Geophys Res 2001;106(D15):17267–92.
[19] Zhang Z, Platnick S, Yang P, Heidinger AK, Comstock JM. Effects of ice particle size vertical inhomogeneity on the passive remote sensing of ice clouds. J Geophys Res 2010;115:D17203. http://dx.doi.org/10.1029/2010JD013835.
[20] Kalashnikova OV, Garay MJ, Davis AB, Diner DJ, Martonchik JV. Sensitivity of multi-angle photo-polarimetry to vertical layering and mixing of absorbing aerosols: quantifying measurement uncertainties. J Quant Spectrosc Radiat Transfer 2011;112:2149–63.
[21] Moré J. The Levenberg–Marquardt algorithm: implementation and theory. In: Watson GA, editor. Lecture Notes in Mathematics: Numerical Analysis, Proceedings of the Biennial Conference Held at Dundee, vol. 630. Berlin: Springer-Verlag; 1977. p. 105–16.
[22] Moré JJ, Garbow BS, Hillstrom KE. User guide for MINPACK-1. Argonne National Laboratory Report ANL-80-74, Argonne, IL; 1980.
[23] Waquet F, Cairns B, Knobelspiesse K, Chowdhary J, Travis LD, Schmid B, et al. Polarimetric remote sensing of aerosols over land. J Geophys Res 2009;114:D01206. http://dx.doi.org/10.1029/2008JD010619.
[24] Mie G. Beigrade zur optik truber medien, speziell kolloidaler metallosungen. Ann Phys (Leipzig) 1908;25:377–455.
[25] Mishchenko MI, Travis LD, Lacis AA. Scattering, absorption, and emission of light by small particles. Cambridge: Cambridge University Press; 2002.
[26] Hammad A, Chapman S. The primary and secondary scattering of sun light in a plane-stratified atmosphere of uniform composition. Philos Mag 1939;28:99–110.
[27] Lenoble J, Herman M, Deuzé JL, Lafrance B, Santer R, Tanré D. A successive order of scattering code for solving the vector equation of transfer in the earth's atmosphere with aerosols. J Quant Spectrosc Radiat Transfer 2007;107:479–507.
[28] Hu Y, Wielicki B, Lin B, Gibson G, Tsay SC, Stamnes K. δ-Fit: A fast and accurate treatment of particle scattering phase functions with weighted singular-value decomposition least-squares fittingJ Quant Spectrosc Radiat Transfer 2000;65:681–90.
[29] Alexandrov MD, Cairns B, Emde C, Ackerman AS, van Diedenhoven B. Accuracy assessments of cloud droplet size retrievals from polarized reflectance measurements by the research scanning polarimeter. Remote Sensing Environ 2012;125:92–111.